Conformational Flexibility, Hydration and State Parameter Fluctuations of Fibroblast Growth Factor-10: Effects of Ligand Binding

Tim J. Kamerzell,[‡] Jay R. Unruh,[§] Carey K. Johnson,[§] and C. Russell Middaugh*[,‡]

Department of Pharmaceutical Chemistry, University of Kansas, Lawrence, Kansas 66047, and Department of Chemistry, University of Kansas, Lawrence, Kansas 66047

Received August 22, 2006; Revised Manuscript Received October 17, 2006

ABSTRACT: Differential effects of ligand binding on local and global fibroblast growth factor-10 (FGF-10) flexibility and stability have been investigated utilizing a variety of experimental and computational techniques. Normal mode analysis was used to predict the low frequency motions and regional flexibility of FGF-10. Similarly, regional variations in local folding/unfolding equilibria were characterized with the COREX/BEST algorithm. Experimental adiabatic and isothermal compressibilities of FGF-10 alone and in the presence of polyanions are compared. Furthermore, the effect of polyanions on the coefficient of thermal expansion is compared. Measurements of density, heat capacity, compressibility, and expansibility were combined to calculate experimentally determined volume and enthalpy fluctuations. Global effects of polyanions on FGF-10 flexibility, thermodynamic fluctuations, and hydration vary depending on the size and charge density of the polyanion. Local effects of polyanions were investigated utilizing time-resolved fluorescence spectroscopy and red edge excitation spectroscopy (REES). Increased rigidity of the protein matrix or an increased solvent response surrounding the Trp residues is observed in the presence of polyanions. Similarly, time-resolved spectroscopy reveals increased ground state heterogeneity and increased dipole relaxation on the time scale of fluorescence for FGF-10 in the presence of polyanions. These polyanions increase heterogeneity, global flexibility, and fluctuations while increasing the melting temperature (T_m) of FGF-10.

It is now generally accepted that protein molecules are not static entities but are more accurately described as dynamic in nature. The dynamic nature of protein molecules covers a broad range of motion from atom fluctuations and side chain oscillations to large scale domain motions (*1*). Furthermore, the timescales of motions that proteins exhibit range from minutes to femtoseconds with energy differences of calories to hundreds of kilocalories and amplitudes ranging from sub-angstrom to hundreds of angstroms (*1*).

A protein in solution may be described as a statistical distribution of microstates with variable degrees of local unfolding, conformational fluctuations, and differential flexibility (*2*−*6*). Protein dynamics may be represented by global harmonic oscillations, global dispersive motions, and/or local anharmonic, random fluctuations of individual atoms or groups. Both local and global conformational fluctuations and flexibility are thought to be important for protein function and stability. Although it is now well established that these broad ranges of motion occur with differential distributions of regional flexibility, our understanding of their biological role in stability, cell communication, catalysis, and so forth is incomplete.

The interaction of ligands with proteins has been shown to modulate both static and dynamic aspects of protein structure, function, and stability. Hilser et al., have shown that ligand induced changes in the loop region of the SH3 domain of Sem 5 result in decreased dynamic character while maintaining some degree of conformational flexibility (*7*). As indicated above, the bound and unbound states represent an ensemble of states rather than discrete conformations. It has been proposed that changes in local conformational fluctuations due to ligand binding modulate local stability, global transitions, and overall stability (*8*). For example, the presence of ssDNA was shown to decrease local motion and slightly increase the motion of various secondary structural elements of *E. coli* topoisomerase I (*9*).

The addition of highly negatively charged polyanions has been shown to enhance the physical stability of certain proteins. MacLean et al., have shown that eight different proteins were stabilized by a variety of low molecular weight dianions (*10*). Similarly, the physical stability of human FGF-1 is markedly increased upon addition of heparin (*11*) and sucrose octasulfate (*12*) as well as a myriad of other polyanions (*11*). The interior and exterior of cells can be viewed as a dense network of polyanionic surfaces that are readily accessible to cellular proteins (*13*). A variety of evidence suggests the involvement of nonspecific electrostatic interactions between cellular polyanionic compounds and protein molecules (*10*−*14*). The ability of proteins to bind a wide range of polyanions suggests that such interactions are not highly specific, although they may be of high affinity. Nonspecific in this context means intermediate specificity based on a gradient of electrostatic charge interactions that are a function of relative charge density in

* Corresponding author. Tel: (785) 864-5813. Fax: (785) 864-5814. E-mail: Middaugh@ku.edu.
[‡] Department of Pharmaceutical Chemistry.
[§] Department of Chemistry.

10.1021/bi061712q CCC: $33.50
Published on Web 11/29/2006

contrast to the more usual high, conformationally based structural specificity (*13*). Numerous polyanions have been found to bind and stabilize FGF-1, other FGFs, and tissue plasminogen activators as well as numerous other protein molecules, suggesting that a low degree of specificity may be a common phenomenon (*15*). The thermodynamics of protein interactions with polyanions is most often found to be entropically driven with multiple proteins often binding to a single polysaccharide chain with moderate affinity (unpublished results) (*16*).

Fibroblast growth factor 10 (FGF-10[1]) is a member of the FGF family of structurally related heparin/polyanion binding proteins involved in a variety of physiological and pathological processes including morphogenesis, angiogenesis, and carcinogenesis. In particular, FGF-10 regulates brain, limb, and lung formation (*17*). FGF activity and specificity is modulated by heparin/heparan sulfate binding, whereas heparan sulfate is required for the high affinity binding of FGF to the FGFR. Heparan sulfate also regulates FGF-10 binding to the distal epithelium and subsequent signaling pathways involved in bud formation and epithelial morphogenesis (*18*). Furthermore, it has been shown that FGF-10 binds oversulfated chondroitin sulfate-E (CS-E), which may be a binding partner to various growth factors in the brain during development (*19*).

This work attempts to better understand the effects of polyanion binding on protein flexibility and stability in the FGF-10 system. The polyanions utilized in this work, in decreasing order of molecular weight, include dextran sulfate, heparin, and phytic acid. A framework for viewing FGF-10 regional and global flexibility and stability is provided through computational analysis of the collective motions utilizing normal mode analysis and the COREX/BEST algorithm. Global flexibility and hydration of FGF-10 alone and in the presence of polyanions are empirically analyzed by measurements of adiabatic and isothermal compressibility and coefficients of thermal expansibility as a function of temperature. Compressibility is directly related to fluctuations in volume, thus directly reflecting flexibility properties (*20*). The coefficient of thermal expansion (α) is used as a measurement of enthalpy and volume fluctuations, macromolecule solvation, accessible surface area, and solvent structure. Furthermore, time resolved fluorescence spectroscopy and red edge excitation spectroscopy are utilized to investigate the protein matrix surrounding the tryptophan residues of FGF-10 alone and in the presence of bound polyanions. Finally, the increase in temperature of the thermal unfolding transition (Tm) of FGF-10 alone and upon addition of polyanions was characterized from DSC experiments.

EXPERIMENTAL PROCEDURES

Fibroblast growth factor 10 (FGF-10, KGF-2) was generously provided by Human Genome Sciences (HGS) as the truncated drug substance Repifermin. Dextran sulfate was purchased from Spectrum, whereas heparin and phytic acid were obtained from Sigma. All other chemicals were of reagent grade and were obtained from Sigma (St. Louis, MO) and Fisher Scientific (Pittsburgh, PA).

FGF-10 was received in HGS formulation buffer and stored at −80 °C. All solutions were prepared in 10 mM citrate buffer at pH 6.00 and dialyzed overnight. The presence of citrate provides sufficient polyanionic stabilization to permit the protein solutions to be easily handled. The dialyzed protein solution was centrifuged for 5 min at 14,000 rpm to remove the aggregated protein before concentration determination. Protein concentration was determined at room temperature by an absorbance measurement at 280 nm (A_{280} nm = 0.65 at 1 mg/mL) using an Agilent 8453 UV-Visible spectrophotometer (Palo Alto, CA) fitted with a Peltier temperature controller. The concentrations used in fluorescence experiments were 0.05−0.1 mg/mL FGF-10 and 2× wt. ratio polyanion. The concentrations used in all other experiments were 2.6−3.4 mg/mL FGF-10 and 2× wt. ratio polyanion.

Normal Mode Analysis. A very powerful theoretical tool for studying collective motions in macromolecules is normal mode analysis (NMA). NMA calculations are based on a harmonic approximation of the potential energy function around a minimum energy conformation. This approximation allows the solution of the equations of motion to be obtained. A protein's normal modes characterize the flexibility and motions around the lowest energy conformation. In proteins, the lowest frequency normal modes generally describe slow, large amplitude motions of functional significance. Two web based servers, ElNemo (*21*) and WebNM@ (*22*), were used to compute and analyze the low frequency normal modes of FGF-10.

The elastic network model (ElNemo), provides an analysis of the dynamic behavior of macromolecules (*21*). ElNemo implements a rotation translation block approximation (*23*), computing the 100 lowest frequency modes and produces residue distance fluctuation maps and the correlation between observed and normal-mode-derived atomic displacement parameters (B-factors). Furthermore, the X, Y, Z eigenvectors are computed from the solution of the equations of motion solved by diagonalizing the Hessian matrix. Therefore, the distributions of the fluctuations driven by the global mode are easily visualized. Suhre et al. provide a more complete description of the methods used to calculate the normal modes via ElNemo (*21*).

WEBnm@ employs a simplified force field for identifying domain dynamics by calculating the energy density associated with local deformations due to the normal modes (*22*). Within this program, normal mode calculations are performed using the MMTK package (*24*). The C-alpha force field is used in which only the C-alpha atoms are assigned the masses of the whole residue they represent. WEBnm@ provides vector field representations, normalized squared atomic displacements, and deformation energies (*22*). This technique is also able to identify both rigid, semi-flexible transition regions and highly flexible domains within a protein matrix.

Protein structure data and atomic parameters were supplied from the Protein Data Bank (PDB) based on the crystal structure analysis of the FGF-10-FGFR2b complex at 2.90

[1] Abbreviations: FGF-10, fibroblast growth factor 10; FGFR, fibroblast growth factor receptor; DS, dextran sulfate; PA, phytic acid; AC, apolar contact; HB, hydrogen bond; HR-US, high resolution ultrasonic spectroscopy; REES, red edge excitation spectroscopy; TRES, time resolved emission spectroscopy; DAS, decay associated spectra; PPC, pressure perturbation calorimetry; DSC, differential scanning calorimetry; NMA, normal mode analysis; CS-E, oversulfated chondroiton sulfate; Tm, thermal melting temperature; HSA, human serum albumin; MEM, maximum entropy method.

Å resolution (*25*). FGFR2b and two *N*-terminal residues were deleted, as is the common practice for normal mode analysis.

Conformational Ensemble and Regional Stability. The COREX/BEST server was employed to generate representations of the thermodynamic conformational ensemble and residue specific stability constants of FGF-10 (*26*). The native structure can be modeled and viewed as distributions of local folding/unfolding conformational fluctuations using the COREX algorithm developed by Hilser et al. (*2*, *26*). An extensive description of the basis of this technique is described elsewhere (*2*, *3*). An empirical validation of this algorithm has previously been demonstrated utilizing hydrogen/deuterium exchange experiments (*3*, *27*). Residue specific stability constants were calculated using COREX/BEST on the basis of the ratio of the summed probabilities of the states in the ensemble for which a residue is in a folded conformation to the summed probabilities of the states for a residue in an unfolded state. Residues with high stability constants are folded in the majority of states, whereas residues with low stability constants are unfolded. The same protein structure data and atomic parameters that were used for NMA were supplied to the COREX/BEST web server.

High Resolution Ultrasonic Spectroscopy (HR-US). All ultrasonic measurements were performed with an HR-US 102 Spectrometer (Ultrasonic Scientific, Dublin, Ireland) with full sample and reference cell volumes (1 mL). The frequencies used for analysis were 5, 7.5, and 12 MHz, whereas the frequency range of the instrument extends from 2 to 18 MHz. The resolution of the HR-US is ± 0.2 mm/s and 0.2% attenuation. Reference cells were filled with buffer or buffer with the appropriate amount of ligand. All solutions were degassed prior to measurement. HRUS v4.50.27.25 software was used for the analysis of all samples. Temperature control was achieved with a Phoenix P2 Circulator (Thermo Haake).

The partial specific adiabatic compressibility of FGF-10 (β_s) was calculated using the following equations

$$\beta_s = -(1/\nu^0)(\partial\nu^0/\partial P)_s = (\beta_0/\nu^0)\lim_{c\to 0}(\beta/\beta_0 - V_0)/c \quad (1)$$

where

$$V_0 = (\rho - c)/\rho_0$$
$$\nu^0 = \lim_{c\to 0}(1 - V_0)/c \quad (2)$$

where β is the adiabatic compressibility of the solution, β_0 is the adiabatic compressibility of the solvent, ρ is the density of the solution, ρ_0 is the density of the solvent, c is the concentration of protein, V_0 is the apparent volume fraction of solvent in solution, and ν^0 is the partial specific volume of solute. The Laplace equation, $\beta = 1/\rho u^2$, was used to calculate the adiabatic compressibility of the solution (β) and solvent (β_0) from the sound velocity (u) and density (ρ) of the solution and solvent. Similarly, the isothermal compressibility (β_T), was calculated by the following equation

$$\beta_T = \beta_s + \alpha^2 T\nu/C_p \quad (3)$$

where T is the absolute temperature, C_p is the specific heat, and α is the thermal expansion coefficient.

Pressure Perturbation Calorimetry (PPC). The heat changes resulting from the pressure changes above each solution were measured with a Microcal VP-DSC microcalorimeter equipped with a PPC accessory (MicroCal, Northampton, MA). A detailed description of this technique is provided elsewhere (*28*, *29*). Briefly, the coefficient of thermal expansion (α) is related to the pressure coefficient of the heat exchange $(\partial Q/\partial P)_T$ through the following relationships

$$\left(\frac{\partial Q}{\partial P}\right)_T = T\left(\frac{\partial S}{\partial P}\right)_T \quad (4)$$

using Maxwell's relationship

$$\left(\frac{\partial S}{\partial P}\right)_T = -\left(\frac{\partial V}{\partial T}\right)_P \quad (5)$$

and substituting

$$\left(\frac{\partial Q}{\partial P}\right)_T = -T\left(\frac{\partial V}{\partial T}\right)_P = -TV\alpha \quad (6)$$

where V is the volume, T is temperature, and α is the coefficient of thermal expansion: $\alpha = (1/V)(\partial V/\partial T)_P$. Reference and sample cells were filled with identical volumes (0.5 mL). Applied pressures were ~5 atm. An average of 15 pressurization and 15 de-pressurization peaks from each of three separate experiments were integrated and used to calculate the coefficient of thermal expansion over the temperature range 20−70 °C.

Differential Scanning Calorimetry (DSC). Absolute heat capacities were measured using a Microcal VP-Capillary DSC with an autosampler (MicroCal, Northampton, MA) and calculated using Microcal subroutines. Experimentally measured partial specific volumes and coefficients of thermal expansion from 20 to 40 °C were included in the calculation. Reference cells contained the appropriate amount of ligand and were subtracted. A total of three separate scans were averaged.

Analysis of State Parameter Fluctuations. Any probability distribution, P_i, can be determined in terms of its mean and the moments about the mean for any parameter X_{ji} (volume, energy) in state i, $\langle X_j\rangle = \Sigma P_i X_{ji}$. Mean square volume fluctuations and enthalpy fluctuations for the second moments of the distribution are given by the following equations (*5*, *20*).

$$\langle \delta V^2\rangle = -kT\left(\frac{\partial V}{\partial P}\right)_{T,\mu_i} = kTV\beta_T \quad (7)$$

$$\langle \delta H^2\rangle = kT^2 C_p \quad (8)$$

Higher moments leading to the calculation of the actual distribution function may be obtained from the lower moments. Second moments describe mean square deviations and the width of the probability distribution, whereas the higher moments depend on the shape and symmetry. Similarly, mixed moments are required to describe fluctuations in more than one state parameter. The mixed moment of volume and enthalpy fluctuations was calculated using the following equation

$$\langle \delta H \delta V\rangle = k_B T^2 V\alpha \quad (9)$$

where k_B is the Boltzmann's constant, V is the volume, and α is the coefficient of thermal expansion. The isothermal compressibility (β_T) of FGF-10 is negative; therefore, the volume fluctuations were not calculated for FGF-10 alone. In the presence of polyanions, however, β_T is positive, and volume fluctuations were calculated.

Density Measurements. Density measurements were performed using a precision density meter, DMA-5000 (Anton Paar, Graz, Austria), with a repeatability of 1×10^{-6} g/cm^3 and 0.001 °C. Solvent and sample solution densities were measured at 2.5 °C intervals from 20 to 40 °C. The density meter was adjusted with dry air and water for all temperatures prior to analysis.

Time Resolved Fluorescence. Fluorescence lifetime decays were measured using the time correlated single photon counting method (*30*). A mode-locked, cavity-dumped Mira Optima 900f Ti:Sapphire system pumped by a 10 W Verdi Laser from Coherent, Inc. (Santa Clara, CA) was used. A Sciencetech 9030 monochromator with a bandpass of 8 nm was used. The wavelength of excitation was 300 nm for all measurements, and data were collected at the magic angle with an Oriel 27320 polarizer. The number of counts in the peak channel was ~30,000 counts for all measured decays.

The fluorescence decays for tryptophan-containing proteins are complex and, therefore, often require a distributed fitting method allowing for non-Gaussian distributions of lifetimes. The maximum entropy method (MEM) described by Livesey and Brochon was used (*31*). This method fits the data to a distribution of fixed, logarithmically spaced lifetimes by minimizing the amplitude surface for the distribution. MEM relies not only on the minimization of the chi-squared statistic but also on the maximization of the entropy function, $S = \Sigma\alpha_i \log \alpha_i$, where S is the informational entropy, and α_i is the amplitude of lifetime component i. Maximization of this function is equivalent to maintaining as little modulation in the amplitude surface as possible. Therefore, this method eliminates the presence of sharp features if they are unwarranted in the data analysis. Hence, if a distribution demonstrates two maxima, then at least two maxima are present in the system, though there may be more that cannot be resolved in the analysis. The algorithm for maximizing the entropy while minimizing the chi-squared is given in detail by Skilling and Bryan (*32*), and we have followed the recommendations of Swaminathan and Periasamy (*33*) in the appropriate data collection procedures for such analysis. At low wavelengths, a scatter component is present at very short times. The scatter component is eliminated in the analysis, and the MEM distributions are cut off at short times; therefore, they do not show this component.

The average fluorescence lifetimes $\langle\tau\rangle$ were calculated directly from the decays using the following equation

$$\langle\tau\rangle = \int_0^\infty t \times I(t)dt / \int_0^\infty I(t)dt \quad (10)$$

where $I(t)$ is the time dependent intensity.

Time Resolved Emission Spectra (TRES). TRES were obtained indirectly by measurement of the time resolved lifetime decays at 10 nm intervals across the emission spectrum from 330−430 nm ($I(\lambda,t)$). The normalized intensity decay functions are given by

$$I'(\lambda,t) = H(\lambda)I(\lambda,t) = \sum_i \alpha_i'(\lambda) \exp[-t/\tau_i(\lambda)] \quad (11)$$

where $\alpha_i'(\lambda) = H(\lambda)\alpha_i(\lambda)$ and

$$H(\lambda) = F(\lambda) / \sum_i \alpha_i(\lambda)\tau_i(\lambda)$$

where $F(\lambda)$ is the steady-state fluorescence spectrum.

Analysis of TRES. The time dependent spectral shifts were characterized by the time dependent center of gravity, which is proportional to the average energy of the emission. The center of gravity is defined by

$$\bar{\nu}_{cg}(t) = \int_0^\infty I'(\bar{\nu},t)\bar{\nu}d\bar{\nu} / \int_0^\infty I'(\bar{\nu},t)d\bar{\nu} \quad (12)$$

where $I'(\bar{\nu},t)$ represents the number of photons per wavenumber interval (*34*). Additional analysis of the spectral relaxation involved the calculation of the time dependent spectral half width defined by the following equation.

$$[\Delta\bar{\nu}(t)]^2 = \int_0^\infty [\bar{\nu} - \bar{\nu}_{cg}(t)]^2 I'(\bar{\nu},t)d\bar{\nu} / \int_0^\infty I'(\bar{\nu},t)d\bar{\nu} \quad (13)$$

Red Edge Excitation Spectroscopy. Steady-state fluorescence measurements of the red edge effect were performed using a PTI Quanta Master Spectrophotometer (Lawrenceville, NJ) equipped with a thermostated cuvette holder. The fluorescence excitation wavelength was varied every 1 nm from 290 to 305 nm. Fluorescence emission spectra were collected from 290 to 430 nm. Excitation and emission slits were set at 3 nm, and a 1 cm path length quartz cuvette was used in all experiments. Buffer baselines were subtracted from each spectrum prior to data analysis. Data analysis was performed using Felix (PTI) software. Emission peak positions were determined by first derivative analysis.

RESULTS

Normal Mode Analysis. B-Factors and Distributions of Fluctuations. Protein movements within FGF-10 can be represented as a superposition of the X, Y, and Z eigenvectors of a Hessian matrix computed using ElNemo. Eigenvectors X, Y, and Z for the two lowest normal modes (7 and 8) are shown in Figure 1. Regional variations in protein fluctuations are easily observed. Highly mobile regions include the *N*- and *C*-termini of FGF-10. A variety of Lys and Arg residues as well as Trp-169 are positioned in semi-mobile regions with Trp-79 in a slightly less mobile region.

ElNemo was utilized to compute B-factors from the mean square displacement $\langle R^2 \rangle$ of the lowest frequency normal modes. Figure 1C compares normalized computed and observed crystallographic B-factors, providing a measure of local protein flexibility. Calculated B-factors agree quite well with experimentally observed B-factors, with a few discrepancies likely due to the approximations involved in the calculations and the rigid environment of protein crystal structures. As is easily observed, highly flexible regions include the *N*- and *C*-termini, residues 117−119 and 171−174 including Arg-174. The dynamic behavior of Trp residues 79 and 169 is of direct interest for comparison with fluorescence experiments (see below). Semi-flexible regions include Trp-169 and a variety of Lys and Arg residues, which are thought to be involved in polyanion binding (*35*).

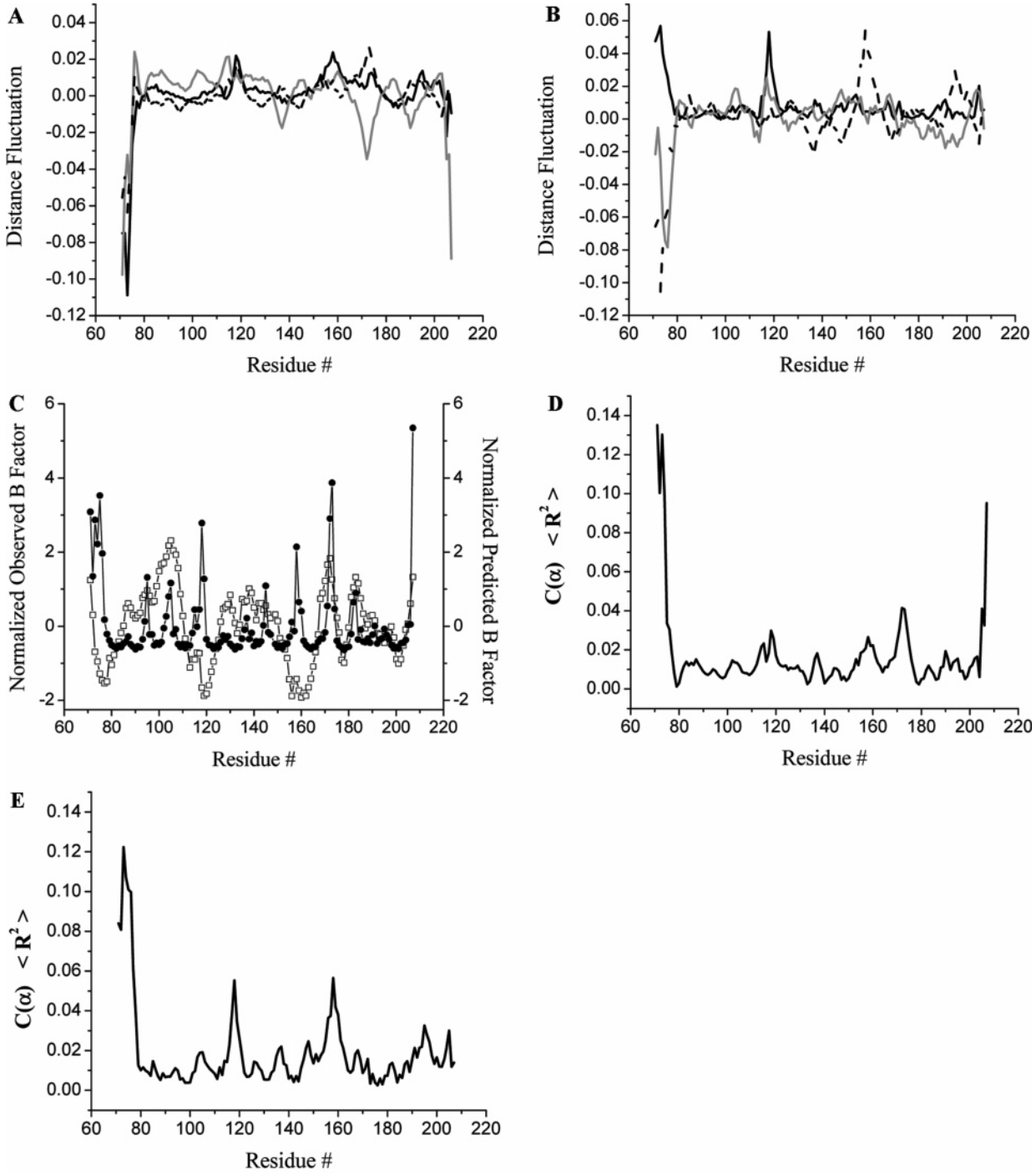

FIGURE 1: Eigenvectors X (black), Y (Gray), and Z (dashed line) displacement map describing the residue distance fluctuations for modes (A) 7 and (B) 8. (C) Normalized predicted (●) and observed (□) crystallographic B-factors. C(α) mean square distance fluctuations for modes (D) 7 and (E) 8.

Tryptophan-169 is expected to exist in a region of limited flexibility as observed by the low B-value, whereas Trp-79 is near the highly flexible *N*-terminus. Similarly, root-mean-square distances between perturbed models and the distributions of fluctuations driven by the lowest frequency modes are shown in Figure 1D and E, respectively.

Porcupine Representation. Porcupine representations are used to describe the direction, amplitude, and relative displacements of the different regions of the protein. Porcupine representations based on normal modes 7 and 8 for FGF-10 are shown in Figure 2.

COREX/BEST Regional Stability. The native conformational ensemble can be modeled and viewed as distributions of local folding/unfolding fluctuations using the COREX algorithm developed by Hilser et al. (*2*, *26*). On the basis of this method, residue specific stability constants are shown for FGF-10 in Figure 3. Residues that are present in regions of folded polypeptide chains in the majority of highly probable states exhibit high stability constants, whereas those residues in unfolded regions in highly probable states are described by low stability constants. Low stability constants are observed for the terminal ends and residues 93−111 of

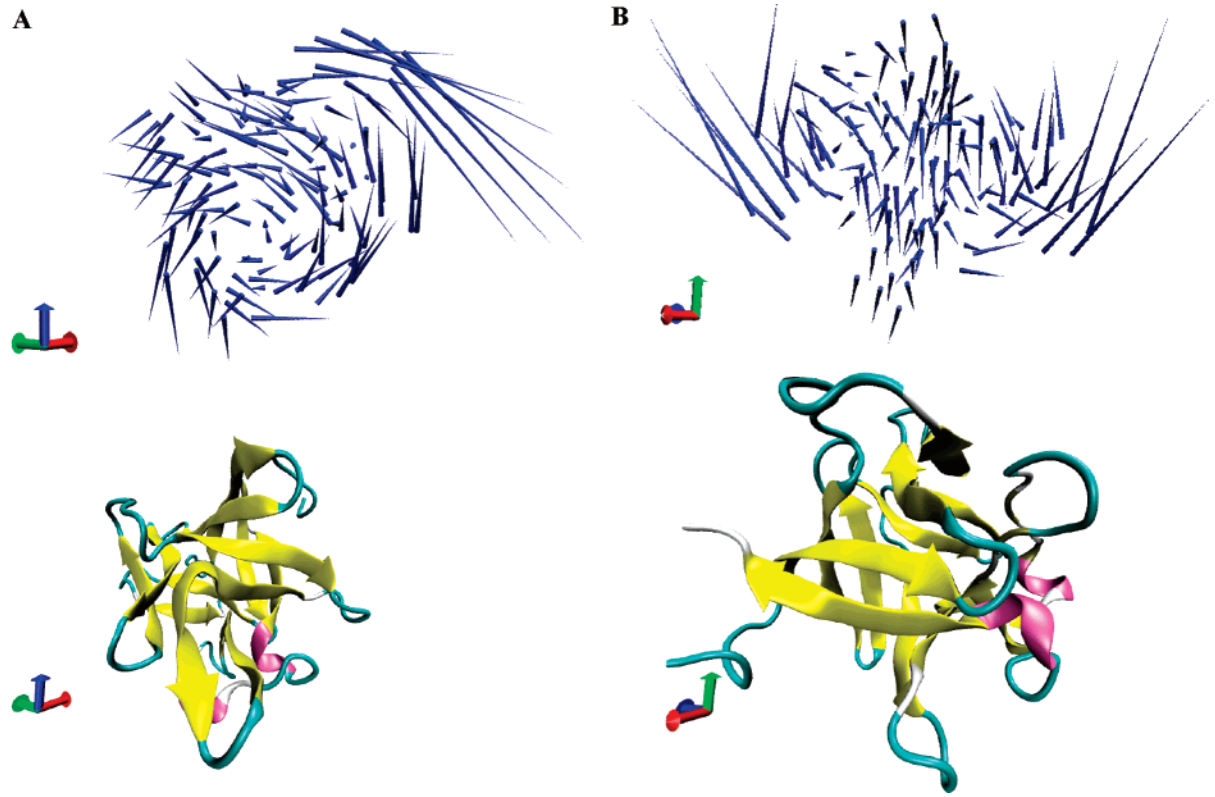

FIGURE 2: Porcupine representation with cones representing the direction and displacements of the regions of the protein for modes (A) 7 and (B) 8.

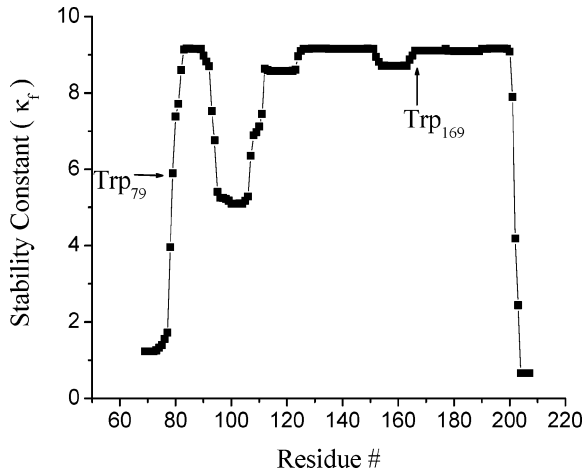

FIGURE 3: Residue specific stability constants of FGF-10 calculated from the COREX/BEST algorithm.

FGF-10, which include Trp-79 and highly conserved residues Arg-78, Arg-80, Lys-81, Lys-91, Lys-94, Lys-97, Lys-124, Lys-153, and Arg-155. High stability constants are observed for a surprisingly large amount of loop regions connecting regular secondary structure elements. Residues of interest that are folded in the majority of highly probably states include Trp-169, Arg-174, Lys-183, Arg-188, Lys-191, and Lys-195.

Adiabatic and Isothermal Compressibility. High resolution ultrasonic spectroscopy measures the velocity and attenuation of high frequency ultrasonic waves as they are passed through a sample. Ultrasonic waves probe intermolecular forces through compressions and decompressions of the material of interest. The elasticity, density, and internal interactions are determined through the measurement of ultrasonic velocity, whereas energy changes in compression and decompression are probed through changes in attenuation of the wave. Attenuation is determined by the scattering of ultrasonic waves in non-homogeneous samples and fast relaxation processes. Protein fluctuations and their coupling to the solvent as well as contribution from compressible cavities and voids in the protein interior can be measured with this technique. The compressibility is directly related to fluctuations in volume, thus reflecting flexibility behavior (*20*).

The relative change in ultrasonic velocity and attenuation between the sample and reference was measured using HR-US. FGF-10 alone and in the presence of various ratios of polyanion display a decrease in relative ultrasonic velocity and increase in absolute velocity as a function of temperature (data not shown). Rigid species possess a higher elastic modulus compared to that of the less rigid species, resulting in a more rapid velocity of sound through the more rigid sample.

Adiabatic (β_S) and isothermal (β_T) compressibility increases as a function of temperature for FGF-10 alone and in the presence of low molecular weight phytic acid (Figure 4A and B). In the presence of the two larger polyanions, heparin and dextran sulfate, FGF-10 adiabatic compressibility increases while the isothermal compressibility decreases from 20 to 40 °C (Figure 4A and B). This temperature range is prior to the protein unfolding transition. β_S is negative over much of the temperature range of interest for FGF-10 alone and in the presence of polyanions. In contrast, β_T is positive over the same temperature in the presence of polyanions and negative for FGF-10 alone. Furthermore, the relative magnitude of β_S and β_T is significantly different at all temperatures for all measured solutions. The magnitude of β_S at all

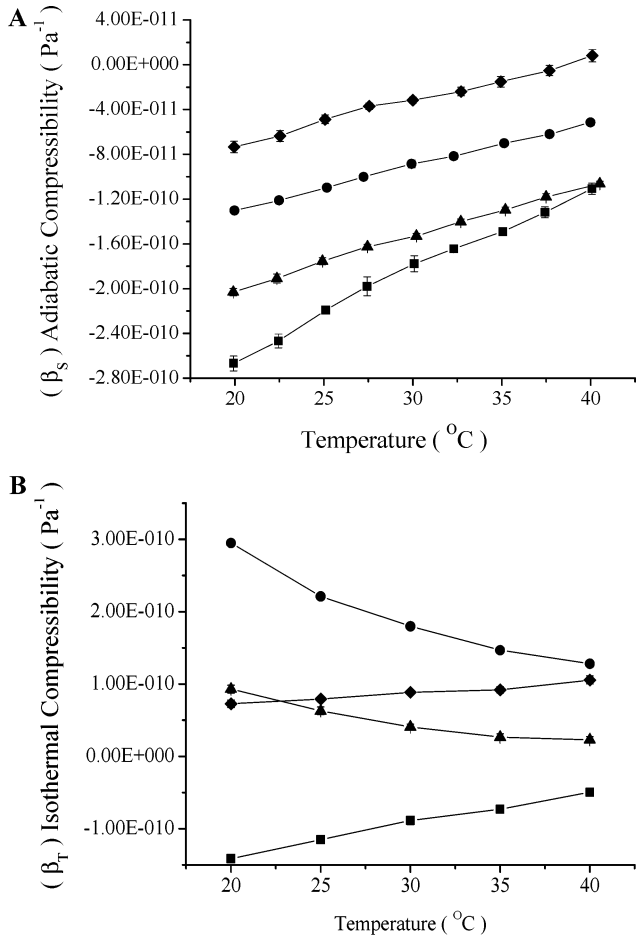

FIGURE 4: (A) Adiabatic and (B) isothermal compressibility of FGF-10 (■), FGF-10 + 2× wt. ratio heparin (▲), FGF-10 + 2× wt. ratio dextran sulfate (●), and FGF-10 + 2× wt. ratio phytic acid (♦) as a function of temperature.

temperatures decreases in the following order: FGF-10 + PA > FGF-10 + DS > FGF-10 + heparin > FGF-10.

Coefficient of Thermal Expansion. Pressure perturbation calorimetry (PPC) measures the heat produced or absorbed when a pressure change is applied simultaneously to a sample and reference cell (*28*). The differential heat change can be used to calculate the thermal coefficient of expansion (α) of the partial volume of the sample. PPC also permits the measurement of macromolecule solvation, accessible surface area, and solvent structure. Large values of α may indicate a greater magnitude of volume fluctuations, a larger magnitude of enthalpy fluctuations, or both (*36*). The addition of ligands and excipients has been shown to modulate the expansibility, volume of unfolding, and the hydration layer of a variety of proteins (*28*).

The coefficient of thermal expansion (α) of FGF-10 alone and in the presence of polyanions was measured using pressure perturbation calorimetry. A decrease in α is observed as a function of temperature for all samples followed by a slight increase near the transition temperature followed by further decreases at higher temperatures (Figure 5). The coefficient of thermal expansion at 20 °C was greatest for FGF-10 in the presence of dextran sulfate followed by FGF-10 in the presence of heparin, phytic acid, and FGF-10 alone. Hydration contributions may be estimated from the relative slope of plots of alpha versus temperature from

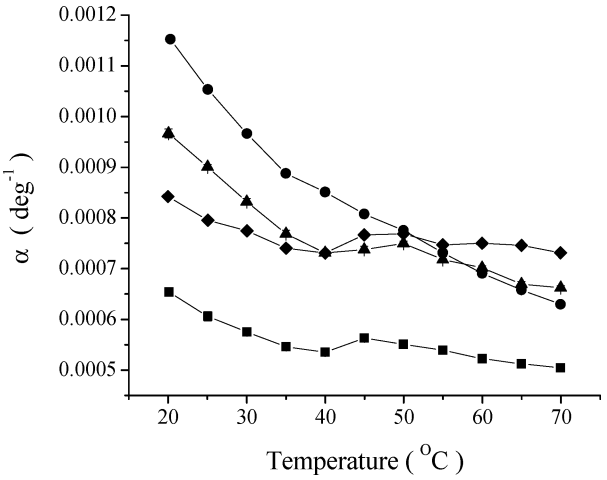

FIGURE 5: Coefficient of thermal expansion of FGF-10 (■), FGF-10 + 2× wt. ratio heparin (▲), FGF-10 + 2× wt. ratio dextran sulfate (●), and FGF-10 + 2× wt. ratio phytic acid (♦) as a function of temperature.

Table 1: Slope ($\Delta(\alpha)/\Delta T_{20-40°C}$) of the Coefficient of Thermal Expansion as a Function of Temperature from 20 to 40 °C for FGF-10 Alone and in the Presence of Polyanions

	$\Delta(\alpha)/\Delta T_{20-40°C}$[a]
FGF-10	−6.0E-6
FGF-10 + phytic acid	−5.6E-6
FGF-10 + heparin	−1.2E-5
FGF-10 + dextran sulfate	−1.5E-5

[a] The error is approximately 1−2%, determined as the coefficient of variation (CV).

20 to 40 °C. The values of $\Delta(\alpha)/\Delta T_{20-40°C}$ for FGF-10 alone and in the presence of polyanions are compared in Table 1.

State Parameter Fluctuations. Enthalpy and volume fluctuations of FGF-10 alone and in the presence of polyanions were calculated from a combination of experimental techniques, including PPC, DSC, HR-US, and density measurements using eqs 7 and 8. Root-mean-square enthalpy fluctuations for FGF-10 alone and in the presence of phytic acid were of similar magnitude, whereas the presence of the much larger polyanions dextran sulfate and heparin significantly decreased $\langle \delta H^2 \rangle^{1/2}$ (Figure 6A). Volume fluctuations decreased as a function of temperature for FGF-10 in the presence of heparin and dextran sulfate (Figure 6B). In the presence of the much smaller polyanion phytic acid, $\langle \delta H^2 \rangle^{1/2}$ increases as a function of temperature. Volume fluctuations for FGF-10 alone were not calculated because of the negative experimental isothermal compressibility. The mixed second moments of enthalpy and volume fluctuations are shown in Figure 6C for FGF-10 alone and in the presence of polyanions. The presence of polyanions increases the mixed moment magnitude $\langle \delta H \delta V \rangle$ in the order of increasing polyanion molecular weight (dextran sulfate > heparin > phytic acid > FGF-10 alone).

Time Resolved Fluorescence. Fluorescence lifetime distributions in proteins are strongly dependent upon the local protein conformation and dynamics. Representative fluorescence lifetime distributions as a function of emission wavelength are shown in Figure 7A and B for FGF-10 alone and FGF-10 in the presence of heparin, respectively. Lifetime distributions of FGF-10 alone as a function of emission wavelength display minimal change. The presence of poly-

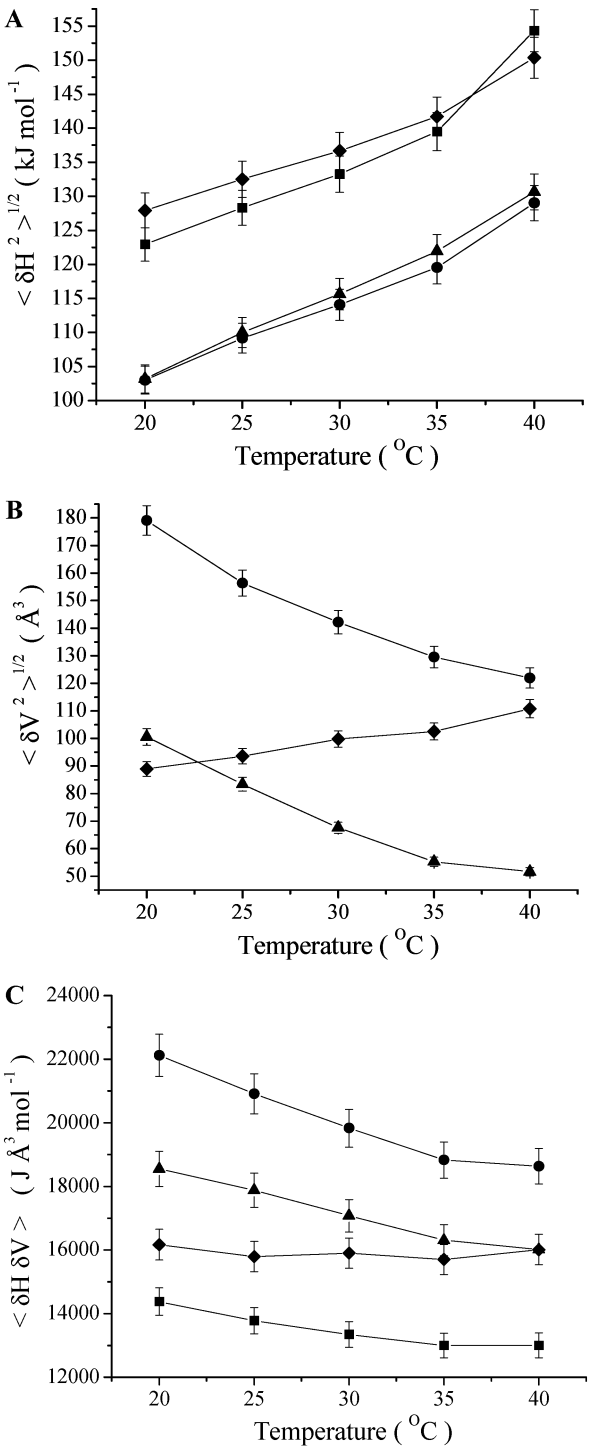

FIGURE 6: Root-mean-square (A) enthalpy, (B) volume, and (C) mixed moment fluctuations of FGF-10 (■), FGF-10 + 2× wt. ratio heparin (▲), FGF-10 + 2× wt. ratio dextran sulfate (●), and FGF-10 + 2× wt. ratio phytic acid (♦) as a function of temperature.

anions, however, dramatically alters the lifetime distributions, which demonstrate significant emission wavelength dependence.

Time resolved emission spectra were reconstructed from the wavelength dependent data (Figure 8A−D). Time dependent spectral shifts were characterized by the time dependent center of gravity, which is proportional to the average energy of the emission (Figure 7E). The change in center of gravity with time is the least for FGF-10 alone, whereas the greatest change is observed with FGF-10 in the presence of heparin. Furthermore, a slight increase in the center of gravity is observed at short times for FGF-10 + heparin and FGF-10 + DS. The presence of each of the polyanions affects the time dependent center of gravity of FGF-10 to varying degrees (Figure 7E).

Additional analysis of the TRES involved the calculation of the time dependent spectral half width (Figure 7D). The spectral width increases modestly as a function of time for FGF-10 alone. An increase to a maximum value followed by a decrease in spectral width with time is observed for FGF-10 in the presence of phytic acid. An increase in spectral width with time to a plateau level is observed for FGF-10 in the presence of the high molecular weight polyanions dextran sulfate and heparin.

Finally, the average fluorescence lifetime $\langle\tau\rangle$ increases as a function of emission wavelength to varying degrees for all samples examined (Figure 7C). The greatest increase was observed for FGF-10 in the presence of heparin. The raw fluorescence emission decays for FGF-10 alone and in the presence of polyanions are shown in the insets of Figure 8A−D.

Red Edge Excitation. Red edge excitation spectroscopy measures the relative rigidity of the protein matrix surrounding the fluorophore(s) of interest. In rigid matrices, the red edge effect is observed because of slow dipole relaxation and site photoselection. Photoselection of the ensemble of species with the strongest solvent fluorophore interaction energies in the excited state is possible when dipole relaxation times are on the same or much longer time scale as the fluorescence lifetimes. If the environment does not change during emission, the energy of emission of the subensemble selectively excited will be lower than the mean of the distribution, and the emission spectra will be shifted toward longer wavelengths resulting in excitation wavelength dependent spectra. An excellent review of this topic is presented by Demchenko (*37*).

The red edge effect probes the dynamics of the redistribution of fluorophores between different environments and reports on local flexibility. FGF-10 alone did not display red edge effects (Table 2). Significant excitation wavelength dependence of the emission maximum was observed in the presence of excess wt. ratios of dextran sulfate (3.9 nm) and heparin (5.7 nm) (Table 2). The emission wavelength dependence of FGF-10 + phytic acid is approximately 1.7 nm.

DISCUSSION

The effects of ligand binding on protein dynamics and stability are incompletely understood. Molecular flexibility and protein motions are important characteristics of protein stability and function. Attempts have been made to correlate protein flexibility and stability with the general finding that decreasing protein motions and/or flexibility can lead to increases in stability (*38*). Such losses in internal flexibility are often found to slow the rate of various forms of chemical degradation as well. For example, the decreased flexibility of recombinant human lymphotoxin was partly responsible for the stabilization of a particular Asn residue by prevention of the adoption of a conformation necessary for cyclic amide formation and subsequent deamidation (*39*). Several examples exist of this phenomenon.

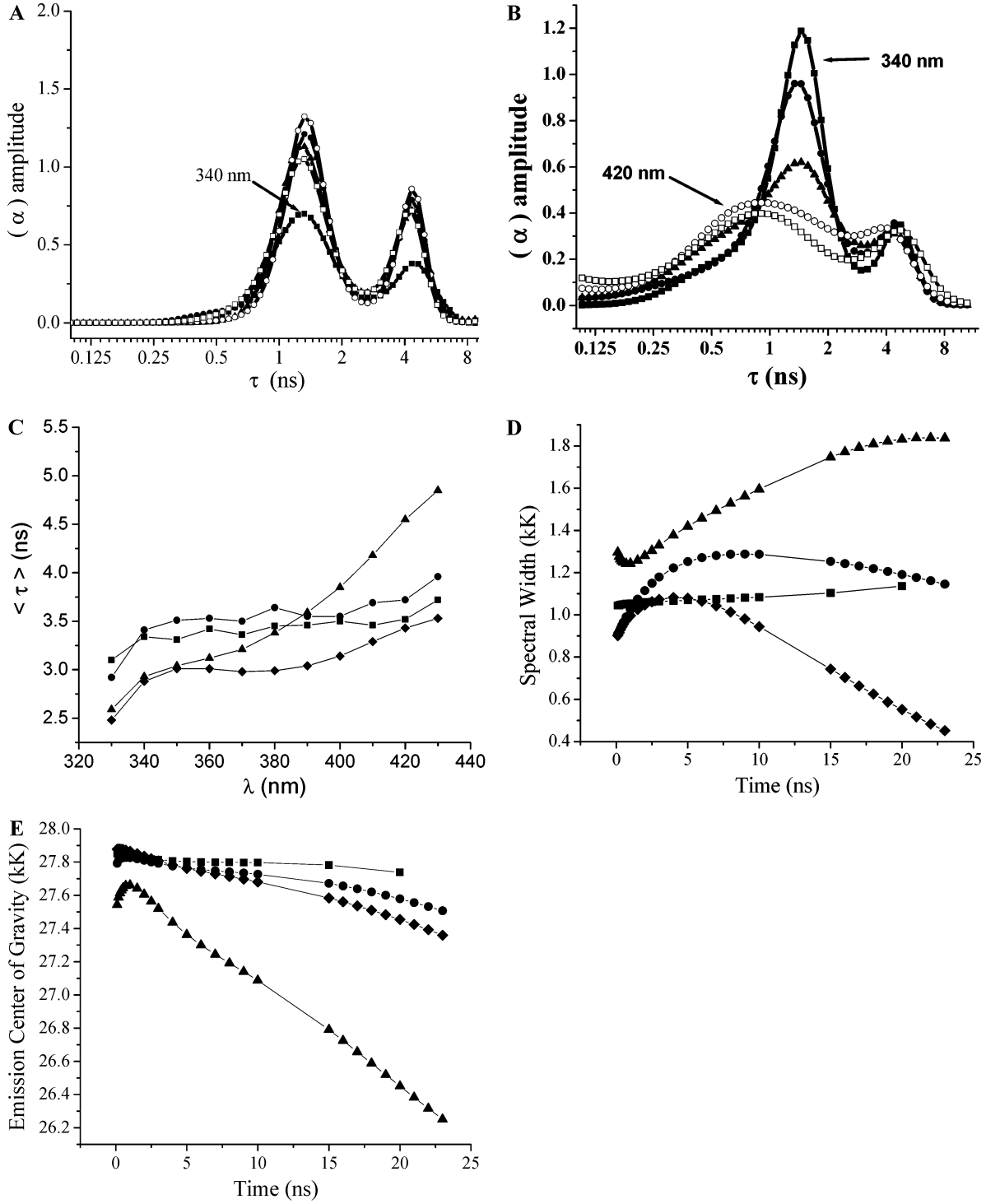

FIGURE 7: Representative fluorescence lifetime distributions of (A) FGF-10 and (B) FGF-10 + heparin as a function of emission wavelength (■) 340 nm, (●) 360 nm, (▲) 380 nm, (○) 400 nm, and (□) 420 nm. (C) Average fluorescence lifetime as a function of emission wavelength of FGF-10 (■), FGF-10 + 2× wt. ratio heparin (▲), FGF-10 + 2× wt. ratio dextran sulfate (●), and FGF-10 + 2× wt. ratio phytic acid (♦). Spectral width (D) and emission center of gravity in kilokaysers (E) of FGF-10 (■), FGF-10 + 2× wt. ratio heparin (▲), FGF-10 + 2× wt. ratio dextran sulfate (●), and FGF-10 + 2× wt. ratio phytic acid (♦) as a function of time.

Observations have been presented, however, that demonstrate increased thermal stability of proteins without increased conformational rigidity (*4*). The increased stability with increased flexibility may originate from positive contributions to the entropy component of ΔG. Increased thermal stability of rubredoxin hybrids was accompanied by increased global flexibility and spatial variations of conformational dynamics compared to the enzymes mesophilic counterparts (*4*). This study probes both the local and global effects of polyanion binding on protein flexibility and stability, a phenomenon of potential functional significance given the role of such ligands in the activity of this class of growth factors (*40*).

Computational analysis suggests that FGF-10 is highly dynamic (Figures 1−3). The *N*- and *C*-termini are the most flexible and dynamic regions of this globular protein. Additional highly mobile and flexible regions include

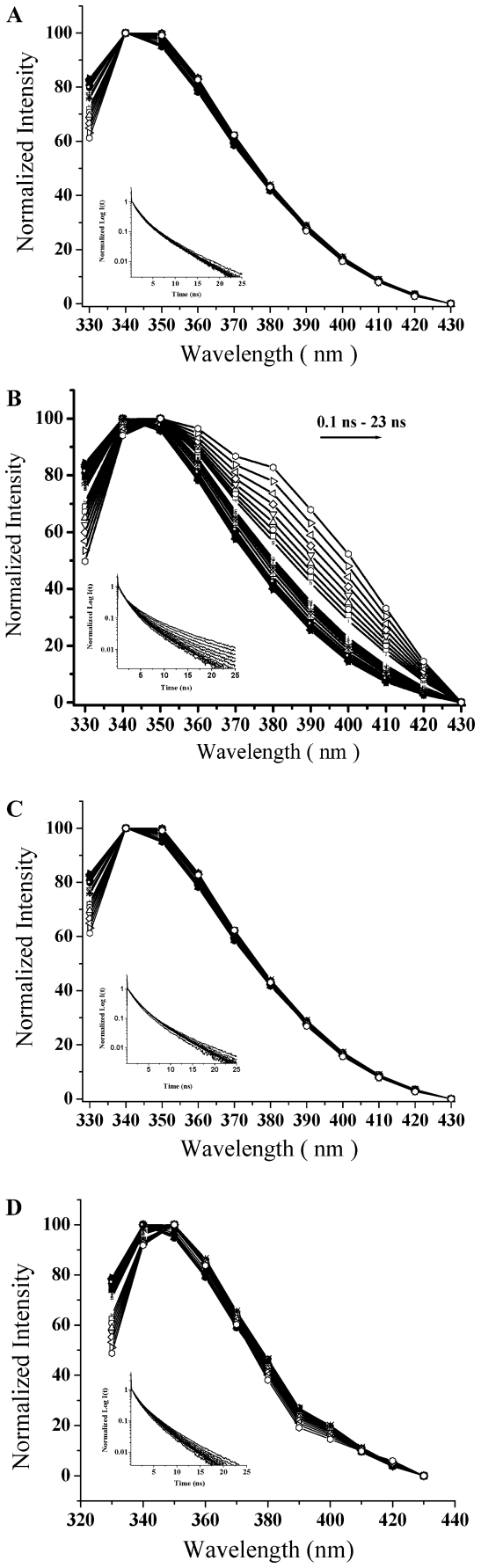

FIGURE 8: Time resolved emission spectrum from 0.1−23 ns of (A) FGF-10, (B) FGF-10 + heparin, (C) FGF-10 + dextran sulfate, and (D) FGF-10 + phytic acid. The insets of A−D are the raw fluorescence emission decays from 330−430 nm.

Table 2: Relative Change in Fluorescence Emission Maximum as a Function of Excitation Wavelength

	$\Delta\lambda_{\text{em. max}\rightarrow 290-305\text{exc.}\lambda}$
FGF-10	0 nm
FGF-10 + phytic acid	1.7 ± 1.0 nm
FGF-10 + dextran sulfate	3.9 ± 0.3 nm
FGF-10 + heparin	5.7 ± 0.4 nm

residues 117−119, 171−174, and Arg-174. The majority of polyanion binding residues (*35*) occur in semi-flexible regions, suggesting the possibility of alteration of local dynamics upon ligand binding. It seems plausible, however, that both regional increases and decreases in flexibility of FGF-10 would occur upon polyanion binding by coupling through the protein matrix.

Experimental adiabatic compressibility (the change in partial specific volume with pressure) values are composed of a hydration $\Delta\nu_{sol}$ and cavity ν_{cav} contribution, as expressed by the following equation.

$$\beta_s^\circ = -(1/\nu^\circ)[\partial\nu_{cav}/\partial P + \partial\Delta\nu_{sol}/\partial P] \qquad (14)$$

β_s° is the result of (1) a positive intrinsic compressibility term, which results from packing defects and cavities in the protein interior, and (2) a negative hydration term, which represents a decrease in the solvent compressibility because of the interactions of water molecules with the solvent exposed groups of the protein (*41*, *42*). Depending on the magnitude of either effect, β_s° may be positive or negative.

The hydration contribution is largest for FGF-10 alone followed by decreased hydration when polyanions are bound (Figure 4). The cavity contribution and compressible void volume is greatest when polyanions bind FGF-10 suggesting increased global deformation and flexibility. It should be pointed out that compressibility is an interplay of both hydration and cavity formation.

Isothermal compressibility measurements reflect volume fluctuations. The direct measurement of β_T has previously been difficult for protein systems. Typically, computer simulations, hole burning, and fluorescence line-narrowing spectroscopy are used to obtain isothermal compressibility. In this work, β_T is calculated on the basis of measurements from a combination of experimental techniques, including HR-US, PPC, DSC, and densitometry. Isothermal compressibility is positive for FGF-10 in the presence of polyanions and negative for FGF-10 alone, suggesting increased protein compressibility when polyanions are bound (Figure 4B). Slow structural relaxation processes contribute to β_T compared to β_S, which reflects hydrational relaxation processes (*43*). The effect of larger polyanions, dextran sulfate and heparin, on FGF-10 structural relaxation as a function of temperature is much greater. The compressibility result in this study is in contrast to the work of Hianik et al. in which human serum albumin (HSA) compressibility is decreased upon the addition of heparin and dextran sulfate (*44*). Furthermore, the hydration of HSA was increased, and the stability decreased in the presence of polyanions (*44*). In contrast, FGF-10 compressibility is increased, hydration is decreased, and stability is increased upon polyanion addition.

The thermal coefficient of expansion is related to the volume and energy fluctuations of the system and is the sum of intrinsic expansivity and hydration contributions (Figure

5). The slope of α versus temperature plots (Table 1) has previously been used as a measure of hydration with a steeper slope indicating greater solvation. The values of the slope found here would seem to indicate a greater extent of FGF-10 hydration in the presence of polyanions, in contrast to the compressibility results. A more probable explanation suggests that α is primarily a result of greater volume fluctuations, in agreement with the compressibility data and calculations involving state parameter fluctuations. Furthermore, molecular dynamics studies have suggested an inverse relationship between the coefficient of thermal expansion and protein stability (*45*). This work provides experimental evidence that this inverse relationship does not necessarily exist. In fact, a more thorough investigation of both local and global flexibility is needed to characterize any system of interest.

Statistical thermodynamics describes fluctuations in state parameters (volume, energy, etc.) based on the second moments of the probability distribution. Even at thermodynamic equilibrium, protein molecules are not static. Calculations of statistical variations from temporal mean values of enthalpy and volume were analyzed on the basis of the experimental measurement of protein compressibility, expansibility, and heat capacity.

Root-mean-square enthalpy fluctuations for FGF-10 in the presence of heparin and dextran sulfate are significantly smaller at all temperatures studied, indicating a narrower probability distribution. A decrease in enthalpy fluctuations of FGF-10 in the presence of polyanions would not necessarily indicate decreased flexibility if two states of very different enthalpies were significantly populated. The maximum in variance (second moment of the distribution) occurs at the midpoint of the themal unfolding transition, and stabilizing the more dynamic state will result in a decrease in enthalpy fluctuations, even though it is more dynamic. Decreased enthalpy fluctuations may also indicate a decreased response to solvent fluctuations. In the presence of polyanions, FGF-10 fluctuations may not be controlled by the solvent to as great an extent as FGF-10 alone. This would not necessarily indicate decreased flexibility of FGF-10 in the presence of polyanions but simply a decreased solvent response. A decreased response to solvent fluctuations may be critical in maintaining protein conformational stability.

Interestingly, volume fluctuations decrease as a function of temperature for FGF-10 in the presence of heparin and dextran sulfate in contrast to increased volume fluctuations with temperature for FGF-10 in the presence of phytic acid (Figure 6B). The observed trend in $\langle \delta H^2 \rangle^{1/2}$ reflects the behavior of β_T with contributions from expansibility, compressibility, hydration, and heat capacity. Therefore, it is inherently difficult to discern the relative contributions to the volume fluctuations as a function of temperature. It is possible that a decrease in volume fluctuations as a function of temperature for FGF-10 in the presence of dextran sulfate and heparin is a result of decreased hydration, compressibility, or both. Volume fluctuations as a function of temperature for FGF-10 in the presence of phytic acid, however, are probably the result of increased compressibility and enthalpy fluctuations.

The mixed second moment of enthalpy and volume fluctuations suggests overall larger fluctuations for FGF-10 in the presence of polyanions with the general trend FGF-10 + DS > FGF-10 + heparin > FGF-10 + PA > FGF-10 alone (Figure 6C). The same trend was observed in stability (T_m) suggesting that in this case, a more flexible protein is more thermostable (Table 3). In fact, the same conclusion that flexible proteins are more thermostable may be drawn from the works of Argos et al. (*46*), Gekko et al. (*41*), and Ponnuswarmy et al. (*47*) on the basis of correlations between T_m, amino acid composition, and compressibility.

Table 3: Midpoint Temperature of the Thermal Unfolding Transition (T_m)

	T_m (°C)
FGF-10	47.42 ± 0.06
FGF-10 + phytic acid	49.29 ± 0.04
FGF-10 + heparin	49.77 ± 0.04
FGF-10 + dextran sulfate	51.72 ± 0.04

Significant difficulty arises when attempting to interpret FGF-10 fluorescence data due to the presence of two Trp residues. As previously stated, Trp-79 is exposed in the majority of highly probable states, whereas Trp-169 is buried in the majority of highly probable states. The computed residue specific stability constants suggest that Trp-79 resides in a more flexible region (Figure 3). An integrated bioinformatics software program, STING Millenium Suite (*48*), was employed to investigate the environment of Trp-79 and -169. Trp-169 forms a total of 10 internal contacts including one apolar contact (AC) with Asn-135, two ACs with Met-176, three ACs with Lys-136, one hydrogen bond (HB) with Met-134, one HB with Ser-166, and two HBs with Asp-149. No internal contacts were observed for Trp-79. Furthermore, Trp-79's solvent accessible surface area (125.25) is significantly greater than that of Trp-169 (78.85) (*48*, *49*).

Time resolved fluorescence spectroscopy of tryptophan provides information on local reorientational dynamics, dipole relaxation, ground state heterogeneity, and time dependent processes. FGF-10 tryptophan fluorescence lifetime distributions suggest an increased ground state heterogeneity in the presence of polyanions (Figure 7A). The distribution of fluorescence lifetimes of FGF-10 in the presence of polyanions manifests a distribution of environments as observed by a broader MEM distribution (Figure 7B). The TRES of FGF-10 in the presence of polyanions (heparin and DS) may be rationalized on the basis of the presence of multiple populations of the more exposed Trp (Figure 8A−D). One population of the more exposed indole (the most probable candidate to interact with polyanions) may be quenched because of the interaction with them. Thus, the rise at <2ns (Figure 7E) with a second population is not quenched, resulting in the long dipolar relaxation times. The MEM distributions seem to suggest such an event. The increase in mean decay time with increasing observation wavelength indicates time dependent spectral relaxation; however, for almost all proteins, the mean decay time increases with increasing emission wavelength (Figure 7C). The presence of heparin affects the Trp environment(s) to the greatest extent. The mechanism of relaxation (i.e., continuous or two state) was not determined because of the complex nature of the decay resulting from the presence of two Trp residues. The greater red edge effect seen for FGF-10 in the presence of heparin (Table 2) implies greater dipolar relaxation due to the reorganization of solvent on the time scale of the fluorescence decay. This result seems to be

consistent with the trends present in the emission center of gravity (Figure 7E). The greater amplitude of the relaxation seen for heparin, rather than the slower time scale, may be the origin of the REE.

CONCLUSIONS

This work provides a unique perspective concerning FGF-10 flexibility and the effects of ligand binding on the protein's dynamics and stability. Perhaps suprisingly, polyanions appear to significantly affect the local environment of tryptophan through the extensive reorganization of the solvent, polyanions, and protein matrix around the indole moieties while increasing global fluctuations and flexibility. It seems probable, however, that polyanion binding increases the rigidity of many residues that are not seen by the methods employed here. Furthermore, polyanions increase the T_m of FGF-10 despite the fact that overall increases in flexibility are observed.

In this case, protein stability does not display a simple inverse correlation between flexibility and stability but rather an interplay of forces resulting from spatial variations in flexibility. Thus, the binding of ligands to proteins will not necessarily increase rigidity but may increase conformational heterogeneity and flexibility. Furthermore, it may be possible that ligand binding increases the number of equilibrium conformational sub-states accessible to the protein while increasing flexibility and stability. Decreasing local destabilizing conformational sub-states, with spatial variations in flexibility and decreased solvent response, may be an important function of many ligands upon substrate binding.

ACKNOWLEDGMENT

We thank Human Genome Sciences for Repifermin and Dr. Periasamy for the use of his maximum entropy program.

REFERENCES

1. Karplus, M., and McCammon, J. A. (1981) The internal dynamics of globular proteins, *Crit. Rev. Biochem. 9*, 293−349; Karplus, M., and McCammon, J. A. (1983) Dynamics of proteins: elements and function, *Annu. Rev. Biochem. 52*, 263−300; Karplus, M., and McCammon, J. A. (1986) The dynamics of proteins, *Sci. Am. 254*, 42−51.
2. Hilser, V. J. (2001) Modeling the native state ensemble, *Methods Mol. Biol. 168*, 93−116; Hilser, V. J., Dowdy, D., Oas, T. G., and Freire, E. (1998) The structural distribution of cooperative interactions in proteins: analysis of the native state ensemble, *Proc. Natl. Acad. Sci. U.S.A. 95*, 9903−9908.
3. Hilser, V. J., and Freire, E. (1996) Structure-based calculation of the equilibrium folding pathway of proteins. Correlation with hydrogen exchange protection factors, *J. Mol. Biol. 262*, 756−772.
4. LeMaster, D. M., Tang, J., Paredes D. I., and Hernandez, G. (2005) Enhanced thermal stability achieved without increased conformational rigidity at physiological temperatures: spatial propagation of differential flexibility in rubredoxin hybrids, *Proteins 61*, 608−616.
5. Cooper, A. (1984) Protein fluctuations and the thermodynamic uncertainty principle, *Prog. Biophys. Mol. Biol. 44*, 181−214.
6. Tang, K. E., and Dill, K. A. (1998) Native protein fluctuations: the conformational-motion temperature and the inverse correlation of protein flexibility with protein stability, *J. Biomol. Struct. Dyn. 16*, 397−411.
7. Ferreon, J. C., and Hilser V. J. (2003) Ligand-induced changes in dynamics in the RT loop of the C-terminal SH3 domain of Sem-5 indicate cooperative conformational coupling, *Protein Sci. 12*, 982−996.
8. Shu, Q., and Frieden, C. (2005) Relation of enzyme activity to local/global stability of murine adenosine deaminase: 19F NMR studies, *J. Mol. Biol. 345*, 599−610.
9. Yu, L., Zhu, C. X., Tse-Dinh, Y. C., and Fesik, S. W. (1996) Backbone dynamics of the C-terminal domain of Escherichia coli topoisomerase I in the absence and presence of single-stranded DNA, *Biochemistry 35*, 9661−9666.
10. Maclean, D. S., Qian, Q., and, Middaugh, C. R. (2002) Stabilization of proteins by low molecular weight multi-ions, *J. Pharm. Sci. 91*, 2220−2229.
11. Volkin, D. B., Tsai, P. K., Dabora, J. M., Gress, J. O., Burke, C. J., Linhardt, R. J., and Middaugh, C. R. (1993) Physical stabilization of acidic fibroblast growth factor by polyanions, *Arch. Biochem. Biophys. 300*, 30−41.
12. Volkin, D. B., Verticelli, A. M., Marfia, K. E., Burke, C. J., Mach, H., and Middaugh, C. R. (1993) Sucralfate and soluble sucrose octasulfate bind and stabilize acidic fibroblast growth factor, *Biochim. Biophys. Acta 1203*, 18−26.
13. Jones, L. S., Yazzie, B., and Middaugh, C. R. (2004) Polyanions and the proteome, *Mol. Cell. Proteomics 3*, 746−769.
14. Burke, C. J., Volkin, D. B., Mach H., and Middaugh, C. R. (1993) Effect of polyanions on the unfolding of acidic fibroblast growth factor, *Biochemistry 32*, 6419−6426; Dabora, J. M., Sanyal, G., and Middaugh, C. R. (1991) Effect of polyanions on the refolding of human acidic fibroblast growth factor, *J Biol. Chem. 266*, 23637−23640.
15. Conrad, H. E. (1998) *Heparin-Binding Proteins*, Academic Press, San Diego, CA.
16. Mach, H., Volkin, D. B., Burke, C. J., Middaugh, C. R., Linhardt, R. J., Fromm, J. R., Loganathan D., and Mattsson, L. (1993) Nature of the interaction of heparin with acidic fibroblast growth factor, *Biochemistry 32*, 5480−5489.
17. Min, H., Danilenko, D. M., Scully, S. A., Bolon, B., Ring, B. D., Tarpley, J. E., DeRose, M., and Simonet, W. S. (1998) Fgf-10 is required for both limb and lung development and exhibits striking functional similarity to Drosophila branchless, *Genes Dev. 12*, 3156−3161; Park, W. Y., Miranda, B., Lebeche, D., Hashimoto G., and Cardoso, W. V. (1998) FGF-10 is a chemotactic factor for distal epithelial buds during lung development, *Dev. Biol. 201*, 125−134; Yokoyama, H., Ide, H., and Tamura, K. (2001) FGF-10 stimulates limb regeneration ability in Xenopus laevis, *Dev. Biol. 233*, 72−79; Clark, J. C., Tichelaar, J. W., Wert, S. E., Itoh, N., Perl, A. K., Stahlman, M. T., and Whitsett, J. A. (2001) FGF-10 disrupts lung morphogenesis and causes pulmonary adenomas in vivo, *Am. J. Physiol.: Lung Cell. Mol. Physiol. 280*, L705−L715; Lovinescu, I., Koyama, E., and Pacifici, M. (2003) Roles of FGF-10 on the development of diathrodial limb joints, *Penn. Dent. J. (Phila.*) *103*, 9.
18. Izvolsky, K. I., Zhong, L., Wei, L., Yu, Q., Nugent M. A., and Cardoso, W. V. (2003) Heparan sulfates expressed in the distal lung are required for Fgf10 binding to the epithelium and for airway branching, *Am. J. Physiol.: Lung Cell. Mol. Physiol. 285*, L838−L846; Izvolsky, K. I., Shoykhet, D., Yang, Y., Yu, Q., Nugent, M. A., and Cardoso, W. V. (2003) Heparan sulfate-FGF10 interactions during lung morphogenesis, *Dev. Biol. 258*, 185−200.
19. Deepa, S. S., Umehara, Y., Higashiyama, S., Itoh N., and Sugahara, K. (2002) Specific molecular interactions of oversulfated chondroitin sulfate E with various heparin-binding growth factors. Implications as a physiological binding partner in the brain and other tissues, *J. Biol. Chem. 277*, 43707−43716.
20. Cooper, A. (1976) Thermodynamic fluctuations in protein molecules, *Proc. Natl. Acad. Sci. U.S.A. 73*, 2740−2741.
21. Suhre, K., and Sanejouand, Y. H. (2004) ElNemo: a normal mode web server for protein movement analysis and the generation of templates for molecular replacement, *Nucleic Acids Res. 32*, W610−W614.
22. Hollup, S. M., Salensminde G., and Reuter, N. (2005) WEBnm@: a web application for normal mode analyses of proteins, *BMC Bioinf. 6*, 52.
23. Tama, F., Gadea, F. X., Marques O., and Sanejouand, Y. H. (2000) Building-block approach for determining low-frequency normal modes of Macromolecules, *Proteins 41*, 1−7.
24. Hinsen, K. (2000) The molecular modeling toolkit: a new approach to molecular simulations, *J. Comput. Chem. 21*, 79−85; Hinsen, K. (1998) Analysis of domain motions by approximate normal mode calculations, *Proteins 33*, 417−429.
25. Yeh, B. K., Igarashi, M., Eliseenkova, A. V., Plotnikov, A. N., Sher, I., Ron, D., Aaronson S. A., and Mohammadi, M. (2003)

Structural basis by which alternative splicing confers specificity in fibroblast growth factor receptors, *Proc. Natl. Acad. Sci. U.S.A. 100*, 2266−2271.
26. Vertrees, J., Barritt, P., Whitten S., and Hilser, V. J. (2005) COREX/BEST server: a web browser-based program that calculates regional stability variations within protein structures, *Bioinformatics 21*, 3318−3319.
27. Whitten, S. T., Garcia-Moreno, E. B., and Hilser, V. J. (2005) Local conformational fluctuations can modulate the coupling between proton binding and global structural transitions in proteins, *Proc. Natl. Acad. Sci. U.S.A. 102*, 4282−4287; Liu, T., Whitten, S. T., and Hilser. V. J. (2005) Ensemble-based signatures of energy propagation in proteins: A new view of an old phenomenon, *Proteins*.
28. Lin, L. N., Brandts, J. F., Brandts J. M., and Plotnikov, V. (2002) Determination of the volumetric properties of proteins and other solutes using pressure perturbation calorimetry, *Anal. Biochem. 302*, 144−160.
29. Plotnikov, V., Rochalski, A., Brandts, M., Brandts, J. F., Williston, S., Frasca V., and Lin, L. N. (2002) An autosampling differential scanning calorimeter instrument for studying molecular interactions, *Assay Drug Dev. Technol. 1*, 83−90.
30. O'Connor, D.V., and Phillips, D. (1984) *Time Correlated Single Photon Counting*. Academic Press, New York.
31. Livesey, A. K. B., J. C. (1987) Analyzing the distribution of decay constants in pulse-fluorimetry using the maximum entropy method, *Biophys. J. 52*, 693; Swaminathan, R., and Periasamy, N. (1996) Analysis of fluorescence decay by the maximum entropy method: influence of noise and analysis parameters on the width of the distribution of lifetimes, *Proc. Natl. Acad. Sci. U.S.A. 108*, 39−49.
32. Skilling, J., and Bryan, R. K. (1984) Maximum entropy image reconstruction: general algorithm, *Mon. Not. R. Astron. Soc. 211*, 111−124.
33. Swaminathan, R., and Periasamy, N. (1996) Analysis of fluorescence decay by the maximum entropy method: influence of noise and analysis parameters on the width of the distribution of lifetimes, *Proc.-Indian Acad. Sci., Chem. Sci. 108*, 39−49.
34. Lakowicz, J. R. (1999) *Principles of Fluorescence Spectroscopy*, Kluwer Academic/Plenum Publishers, New York.
35. Schlessinger, J., Plotnikov, A. N., Ibrahimi, O. A., Eliseenkova, A. V., Yeh, B. K., Yayon, A., Linhardt, R. J., and Mohammadi, M. (2000) Crystal structure of a ternary FGF-FGFR-heparin complex reveals a dual role for heparin in FGFR binding and dimerization, *Mol. Cell 6*, 743−750.
36. Ravindra, R., and Winter, R. (2003) On the temperature−pressure free-energy landscape of proteins, *ChemPhysChem. 4*, 359−365.
37. Demchenko, A. P. (2002) The red-edge effects: 30 years of exploration, *Luminescence. 17*, 19−42.
38. Dill, D. E. S. T. a. K. A. (1998) Native protein fluctuations: the conformational-motion temperature and the inverse correlation of protein flexibility with protein stability, *J. Biomol. Struct. Dyn. 16*, 397−411.
39. Xie, M., Shahrokh, Z., Kadkhodayan, M., Henzel, W. J., Powell, M. F., Borchardt, R. T., and Schowen, R. L. (2003) Asparagine deamidation in recombinant human lymphotoxin: hindrance by three-dimensional structures, *J. Pharm. Sci. 92*, 869−880.
40. Wiedlocha, A., and Sorensen, V. (2004) Signaling, internalization, and intracellular activity of fibroblast growth factor, *Curr. Top. Microbiol. Immunol. 286*, 45−79.
41. Gekko, K., and Hasegawa, Y. (1986) Compressibility-structure relationship of globular proteins, *Biochemistry 25*, 6563−6571.
42. Gavish, B., Gratton E., and Hardy, C. J. (1983) Adiabatic compressibility of globular proteins, *Proc. Natl. Acad. Sci. U.S.A. 80*, 750−754.
43. Smirnovas, V., Winter, R., Funck, T., and Dzwolak, W. (2005) Thermodynamic properties underlying the alpha-helix to beta-sheet transition, aggregation, and amyloidogenesis of polylysine as probed by calorimetry, densimetry, and ultrasound velocimetry, *J. Phys. Chem. B 109*, 19043−19045.
44. Hianik, T., Ponikova, S., Bagel'ova, J., and Antalik, M. (2006) Specific volume and compressibility of human serum albumin-polyanion complexes, *Bioorg. Med. Chem. Lett. 16*, 274−279.
45. Palma, R., and Curmi, P. M. (1999) Computational studies on mutant protein stability: The correlation between surface thermal expansion and protein stability, *Protein Sci. 8*, 913−920.
46. Argos, P., Rossman, M. G., Grau, U. M., Zuber, H., Frank G., and Tratschin, J. D. (1979) Thermal stability and protein structure, *Biochemistry 18*, 5698−5703.
47. Ponnuswarmy, P. K. M. R., and Manavalan, P. (1982) Amino acid composition and thermal stability of proteins, *Int. J. Biol. Macromol. 4*, 186.
48. Neshich, G., Mancini, A. L., Yamagishi, M. E., Kuser, P. R., Fileto, R., Pinto, I. P., Palandrani, J. F., Krauchenco, J. N., Baudet, C., Montagner A. J., and Higa, R. H. (2005) STING Report: convenient web-based application for graphic and tabular presentations of protein sequence, structure and function descriptors from the STING database, *Nucleic Acids Res. 33*, D269−D274; Neshich, G., Rocchia, W., Mancini, A. L., Yamagishi, M. E., Kuser, P. R., Fileto, R., Baudet, C., Pinto, I. P., Montagner, A. J., Palandrani, J. F., Krauchenco, J. N., Torres, R. C., Souza, S., Togawa, R. C., and Higa, R. H. (2004) JavaProtein dossier: a novel web-based data visualization tool for comprehensive analysis of protein structure, *Nucleic Acids Res. 32*, W595−W601; Neshich, G., Togawa, R. C., Mancini, A. L., Kuser, P. R., Yamagishi, M. E., Pappas, G., Jr., Torres, W. V., Fonseca e Campos, T., Ferreira, L. L., Luna, F. M., Oliveira, A. G., Miura, R. T., Inoue, M. K., Horita, L. G., de Souza, D. F., Dominiquini, F., Alvaro, A., Lima, C. S., Ogawa, F. O., Gomes, G. B., Palandrani, J. F., dos Santos, G. F., de Freitas, E. M., Mattiuz, A. R., Costa, I. C., de Almeida, C. L., Souza, S., Baudet, C., and Higa, R. H. (2003) STING Millennium: A web-based suite of programs for comprehensive and simultaneous analysis of protein structure and sequence, *Nucleic Acids Res. 31*, 3386−3392.
49. Lee, B., and Richards, F. M. (1971) The interpretation of protein structures: estimation of static accessibility, *J. Mol. Biol. 55*, 379−400; Tsodikov, O. V., Record, M. T., Jr., and Sergeev, Y. V. (2002) Novel computer program for fast exact calculation of accessible and molecular surface areas and average surface curvature, *J. Comput. Chem. 23*, 600−609.

BI061712Q